Non-linearities and Timescales in Temporal Interference Deep Brain Stimulation

Tom Plovie, Ruben Schoeters, Thomas Tarnaud, Luc Martens, Wout Joseph, Emmeric Tanghe

***Abstract*—*Objective*: In temporal interference (TI) deep brain stimulation (DBS), the neurons of mice react to two interfering sinusoids with a slightly different frequency. This is called a temporal interference (TI) signal. It was previously seen that for the same input intensity, the neurons do not react to a purely sinusoidal signal. This study aims to get a better understanding into the mechanism for this, which is largely unknown. *Methods*: This study makes use of single compartment models to computationally simulate the response of neurons to the sinusoidal and TI-waveform. This study also compares different neuron models to get insight in which models are able to model the experimental behavior. *Results*: It was found that integrate-and-fire models do not reflect the experimental behavior while the Hodgkin-Huxley and Frankenhaeuer-Huxley model do reflect this behavior. It was seen that changing the characteristics of the ion gates in the Frankenhaeuser-Huxley model alters the response to both sinusoidal and TI signal. It can even make sure that the firing threshold of the sinusoidal input becomes lower than that of the TI input. *Conclusion*: The results show that the ion-gates have a big influence on the behavior and their characteristics can define the way the neuron reacts to sinusoidal and TI inputs. *Significance*: This paper makes advances both in terms of biophysical insight of the neuron as well as the insight in computational modelling of TI-stimulation.**

***Index Terms*—Computational neuron models, ion gates, non-linearities, temporal interference deep brain stimulation**

This work was carried out using the Supercomputer Infrastructure (STEVIN) at Ghent University, funded by Ghent University, the Flemish Supercomputer Center (VSC), the Hercules Foundation and the Flemish Government department EWI.

This research was funded by the FWO-project G019121N. T Tarnaud is a postdoctoral Fellow of the FWO-V (Research Foundation Flanders, Belgium). R Schoeters is a PhD Fellow of the FWO-V (Research Foundation Flanders, Belgium).

T. Plovie, R. Schoeters, T. Tarnaud, L. Martens, W. Joseph, E. Tanghe are with the Department of Information Technology (INTEC-WAVES/IMEC), Ghent University/IMEC, Technologypark 126, 9052 Zwijnaarde, Belgium. E-mail: tom.plovie@ugent.be

I. Introduction

NOWADAYS, many applications for brain stimulation exist. One of these applications is deep brain stimulation (DBS) that was mainly developed to treat Parkinson's Disease (PD). DBS is able to reduce the motor symptoms of PD. However it has an important disadvantage: it is invasive and can cause complications (e.g. bleeding in the brain, stroke, infection, ...) [1]. Because of this, a new technique is being developed named temporal interference deep brain stimulation (TI-DBS). With this technique, two sinusoidal electric fields, oscillating at a high but slightly different frequency, are sent into the brain. At the place where they interfere, an amplitude modulated signal is created. This is illustrated in Figure 1. Grossman et al. (2017, 2018) [2], [3] has found from experiments on mice that the neurons respond to this interference pattern but not to the constituting sinusoids separately. Therefore, it is a non-invasive alternative to the conventional, invasive DBS techniques. Although promising, there are still some limitations to overcome before TI-DBS can be used for humans in practice. A first limitation is that the technique has only been tested on mice and not on humans. Secondly, the mechanism in the neuron that allows this type of stimulation is unknown. It is thus very hard to predict if all neuron types in the human brain will react to the stimulation in the same way and thus if this technique would work with humans.

Other experiments in mice have shown that it is possible to cause eye movements at the beat frequency of the TI-signal [4] confirming the importance of the beat frequency. It should be noted that TI-stimulation is not only used in the brain. It was shown in rats that TI-stimulation can activate spinal motor neurons in the neck to restore breathing after opioid overdose. Again it was shown that a single sine waveform is not able to cause stimulation [5]. Furthermore, TI has been studied for retinal stimulation [6].

Instead of using electrodes creating the electric field inside the brain, it is also possible to use TMS coils creating a magnetic field and inducing an electric field. It is possible to achieve a TI-waveform by using the same technique of multiple frequencies [7], [8].

To get more insight in the electric field distribution of TI-DBS in the human brain, finite element simulations have been done. The TI-DBS has been compared to a conventional technique like tACS. This showed that when the same electric field strength is achieved inside the focus you want to stimulate, TI-DBS causes a smaller maximal electric field outside this focus than with tACS [9]. In contrast to the traditional DBS technique, it is easier to steer the stimulation site with TI-

DBS. This can be done by changing the electrode positions or by adjusting the relative amplitudes of the current at the different electrode pairs [9]–[11]. With these degrees of freedom, it it possible to find the optimal electrode position so the electric field is high inside in the region of interest and low outside of it. This optimal electrode positioning is very person specific. With the same electrode positioning, high variations are possible in the simulated electric fields for different people [9]. Huang and Parra (2019) argue that it is possible to achieve sufficienlty high electric fields using tACS. To achieve this, the electrode positioning becomes more important because it makes use of the CSF as a conductor for the electric field. It is thus even more challenging to obtain a patient specific electrode position. They do mention that the focality is still worse with this technique than with TI-stimulation [12]. The focality in TI-stimulation is in the cm-range [13].

Regarding the underlying mechanism in the neuron to allow this stimulation type, one of the earliest hypotheses was that it had to do with the intrinsic low-pass filter properties of a neuron together with a non-linear component of the neuron. Because of this, the neuron can not react to the high frequency oscillations and therefore responds to the low frequent envelope of the TI-signal [2], [3]. It is clear that the low-pass filter property can not be the single explanation because with only the properties of a low pass filter, the envelope could not be extracted by the neuron and it would not respond to the beat frequency. In an alternative idea, the neuron acts as a rectifier and a demodulator. However, this is again not totally correct because high frequency oscillations can still be found in the membrane voltage response [14], [15]. Up to now, it was said that high frequency signals do not cause stimulation. This is not entirely true, there are actually three ways of a neuron to respond to a high frequency signal.

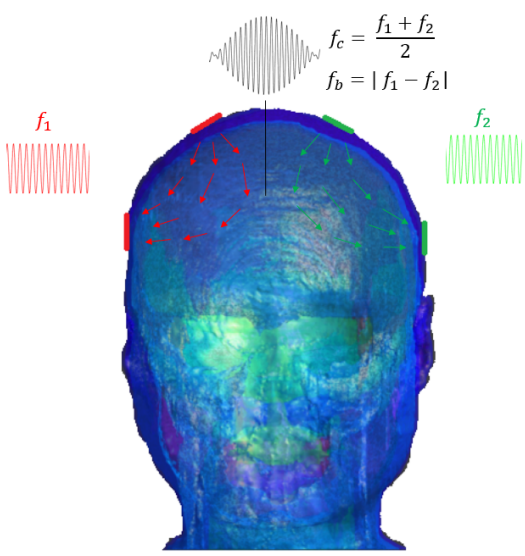

Fig. 1: Schematic of the concept of TI-DBS where the red and green electric field oscillate at a different frequency. At the place where they interfere, the black amplitude modulated signal is created.

There can be one AP at the signal onset, there can be a continuous firing or there can be a depolarization block. It may be impossible to stimulate the deep regions of the brain without also causing a conduction block in other parts of the brain [14]. This conduction block occurs at higher input intensities and could lead to an upper limit for the use of TI-stimulation [2]. It was found in silico and in vivo that increasing the carrier frequency of the TI-signal increases the threshold of the input needed to cause stimulation. Changing the beat frequency did not seem to have an influence on the threshold [2], [11]. To model TI-stimulation, it was found that IF-neurons are not sufficient to reproduce the experimental behaviour on single neuron level [16]. However, when IF-neurons are placed in a network and $\mathrm{GABA_b}$ postsynaptic inhibition is included, the computational results were in line with experimental observations of TI-stimulation [17]. Furhter on, for single cell neurons, it is possible to have neurons exhibiting TI-stimulation when using the FitzHugh-Nagamo model and the Hodgkin-Huxley model. It was also seen that not all mammalian cells exhibit TI [15], [16]. Howell et al. (2021) argues that because of the large dimensions of a human head, TI-stimulation seems unfeasible. However, it is suggested that subthreshold TI-stimulation can be used to synchronise the firing of neurons to the TI-signal. Next to the immediate effect on the neuron, TI-stimulation could also, like other electrical stimulation methods, impact the plasticity and the interconnectivity of neurons [18]. This paper elaborates on the use of computational single cell neurons.

The first novelty of this paper is the demonstration that the non-linearity of the Goldman-Hodgkin-Katz (GHK) equation in the Frankenhaeuser-Huxley model is not strictly required to demonstrate the effect of TI-stimulation found in Grossman et al. (2018) [3] via computational modeling. Secondly, physiologically realistic models (Frankenhaeuser-Huxley and Hodgkin-Huxley) are compared to different integrate-and-fire (IF)- models to determine which aspects in a computational neuron model are needed to show the effect of TI-stimulation. The third novel aspect is the investigation of the different influences of both the time constants and the steady state parameters of the gates to obtain a biophysical explanation of the mechanism of the neuron reacting to TI-stimulation.

II. Methods

A. Neuron models

In this study, single compartment models are used. This means that the morphology of the neuron is not taken into account. The five existing models that are used are the Hodgkin-Huxley (HH) [19], Frankenhaeuser-Huxley (FH) [20], leaky integrate-and-fire model (LIF), exponential integrate-and-fire (EIF) and the adaptive and exponential integrate-and-fire (AdEx) model. The first two are described by the following equations:

$$C_M \frac{dV}{dt} = I_e - (I_l + \sum_X I_X) \tag{1}$$

$$\frac{dx}{dt} = \alpha_x(V)(1-x) - \beta_x(V)x \tag{2}$$

where C_M is the membrane capacitance, V is the membrane potential, I_e is the input current, I_l is the leak current and I_X are the currents linked to voltage dependent gates, where X can be Na, K or p. In (2), x can be m, h, n or p. These are the open probabilities of the respective gates. p is only used in the FH-model. $\alpha_x(V)$ and $\beta_x(V)$ are the open and close rates of the gates and are retrieved from [19] and [20]. For TI, I_e is of the form $I_e = \frac{A}{2}(\sin(2\pi f_1 t) + \sin(2\pi f_2 t)) = A\cos(\pi f_b t)\sin(2\pi f_c t)$, where f_b is the beat frequency and f_c is the carrier frequency.
This equation can be rewritten to

$$\tau_x(V)\frac{dx}{dt} = x_\infty(V) - x \tag{3}$$

where $\tau_x(V)$ and $x_\infty(V)$ are the time constant and the steady state value characterising the gates. The ion currents of the FH-model and HH-model are of the form of (4) and (5), respectively.

$$I_X = m^a h^b n^c p^d P_X \frac{VF^2}{R_\mathrm{g}T}\frac{[X]_o - [X]_i \exp(\frac{VF}{R_\mathrm{g}T})}{1-\exp(\frac{VF}{R_\mathrm{g}T})} \tag{4}$$

$$I_X = m^e h^f n^k g_X(V - E_X) \tag{5}$$

(4) is known as the Goldman-Hodgkin-Katz (GHK) -flux equation. P_X is the ion-specific permeability, F is the Faraday constant, R_g is the ideal gas constant and T is the temperature. The LIF-model is decribed by:

$$\tau_m \frac{dV}{dt} = RI_e - (V - V_r) \tag{6}$$

and the EIF-model is decribed by:

$$\tau_m \frac{dV}{dt} = RI_e - (V - V_r) - \Delta_T \exp\left(\frac{V - V_T}{\Delta_T}\right) \tag{7}$$

where τ_m is the membrane time constant, R is the membrane resistance, V_r is the resting potential, Δ_T is the slope factor that determines the sharpness of the threshold and V_T is the spike threshold. When the threshold V_thresh is reached, the potential resets to V_reset. Note that the LIF-model is the EIF-model in the limit of $\Delta_T \to 0$. The AdEx-model is very similar but has an additional differential equation. It is described by:

$$\tau_m \frac{dV}{dt} = RI_e - (V - V_r) - \Delta_T \exp\left(\frac{V - V_T}{\Delta_T}\right) - RW \tag{8}$$

$$\tau_w \frac{dW}{dt} = a(V - V_r) - W \tag{9}$$

where the additional parameter a determines the level of sub-threshold adaptation. Again when a threshold V_{th} is reached, the potential resets to V_reset while W is changed into $W + b$ [21]. The used parameters for the presented results of the IF-models are given in table I unless stated otherwise.
To investigate the influence of the non-linearity of the GHK-equation, two new models are constructed from the HH- and FH-model. A linearized version of the FH-model (FH1) is obtained by replacing the ion currents by their first order Taylor expansion resulting in the form described by (5). For the HH-model, the opposite is done. It is assumed that the HH-model is the first order Taylor expansion of a more general model. This more general model is then of the form of (4) and is called the gHH-model. In order to obtain these new models, the right points (($V_{Na,0}$, $V_{K,0}$) and ($V_{Na,0}$, $V_{K,0}$, $V_{p,0}$)) for this Taylor expansion should be found for the gHH and FH1 model, respectively. Two methods are followed to realise this, resulting in four derived models: gHHv1, FH1v1 (method 1) and gHHv2, FH1v2 (method).
The first method constists of calculating the reversal potentials for the ion currents (i.e. the Nernst potentials) and taking these as expansion points. In the second method, a sweep is done over several combinations of possible Taylor expansion points. For each set, several combinations of duration and intensity of a rectangular input signal are tested: $I_e = [300, 356, 411, 467, 522, 578, 633, 689, 744, 800]\frac{\mu\mathrm{A}}{\mathrm{cm}^2}$ for the FH-model, $I_e = [0, 11.11, 22.22, 33.33, 44.44, 55.56, 66.67, 77.78, 88.89, 100.0]\frac{\mu A}{cm^2}$ for the HH-model and $t_{dur} = [0.050, 0.27, 0.48, 0.7, 0.92, 1.13, 1.35, 1.56, 1.78, 2.00]\mathrm{ms}$ for both models. For every combination, the correlation between the membrane response of the original and the new model is calculated. The correlations of the different duration-intensity combinations are averaged. The ($V_{K,0}$, $V_{Na,0}$)-combination with the highest average correlation is chosen for the new model. For the FH1 models, it is assumed that $V_{p,0} = V_{Na,0}$

TABLE I: Parameters for the IF-models

V_r	-70 mV
V_reset	-70 mV
V_thresh	-40 mV
R	$0.5 \cdot 10^6 \mathrm{k}\Omega$
τ_m	5 ms
Δ_T	2 mV
V_T	-50 mV
τ_w	$100ms$
a	$2 \cdot 10^{-9}\mathrm{mS}$
b	$8 \cdot 10^{-6}\mu\mathrm{A}$

B. Software

The programming, analysis and simulations were performed in MATLAB R2020a where the ode45, ode15s and ode4 solvers of Matlab were used to calculate the neuron response numerically [22]. The fixed step ode4-solver was for example needed for transforming the signals to the frequency spectrum. The variable step variable order solvers, ode45 and ode15s were used to speed up the simulations when no frequency information was needed. The principle of the ode45 and ode15s, is explained in Ashino et al. (2000) [23].

C. Gates: Time constants

To investigate the influence of the time constants, a small adaptation is made to (2). A parameter k_x is introduced to scale the time constant of the gates so that

$$\tau_{x,new} = k_x \tau_{x,original} \qquad [\mathrm{s}] \tag{10}$$

This results in

$$\frac{dx}{dt} = \frac{\alpha_x(V)}{k_x}(1-x) - \frac{\beta_x(V)}{k_x}x \tag{11}$$

D. Gates: Steady state values

Lastly the steady state values of the gates are investigated in more detail. The equations for the steady state values are replaced by a logistic function like (12), while the original time constant equations are maintained.

$$x_\infty = \frac{1}{1+\exp(-a(V-V_r-b))} \tag{12}$$

The influence of the parameters a and b on the TI-effects can then be investigated. Note that this approximation is purely to get insight in how the behavior changes with changing parameters and not to approximate the real behavior of the neuron globally. V_r is the rest potential and is equal to -70 mV.

E. Analysis

The analysis of the results was done based on the firing rate (FR) and the new energy metric defined below in (14). For the firing rate, first the action potentials (APs) needed to be determined. An AP was detected based on the signal of the m-gate. The m-gate, that is responsible for the Na^+-influx that initiates the AP, needs to cross a threshold value of 0.75 for an AP to be counted. An additional rule is set that the m-gate needs to drop below 0.10 before a new AP can be counted, in order to avoid miscounts when the m-gate oscillates around 0.75. Then the FR is calculated with:

$$\mathrm{FR} = \frac{n}{t_{\mathrm{stim}}} \qquad [\mathrm{Hz}] \tag{13}$$

where n is the number of APs counted and t_{stim} is the duration of the stimulation.

Because the FR seemed to have a disadvantage with highly oscillating signals at higher intensities, a metric based on the energy of the signal is introduced for extra analysis. For highly oscillating signals, a false zone appeared where the FR indicated firing at the beat frequency while the firing was actually a lot faster. The reason is that the m-gate does not always drop below 0.10 in these cases. This metric pTI (percentage of TI) is defined as:

$$\mathrm{pTI} = \frac{\mathrm{E_{TI,b}}}{\mathrm{E_{TI,tot}}} \qquad [-] \tag{14}$$

where $E_{\mathrm{TI,b}}$ is the energy at the beat frequency and the first harmonic of the beat frequency of the response to the TI-signal. $E_{\mathrm{TI,tot}}$ is the total energy in the membrane response to the TI-signal. The total energy is restricted to energies at frequencies higher than 0 Hz.

III. Results

A summery of the most important results is given in Tables II and III. Table II shows for which of the discussed models it is possible to get a a TI-zone. The TI-zone is the range of input intensities for which the TI-signal causes firing at the beat frequency and the sine input with the same carrier frequency does not cause regular firing. Table III shows for which values of the parameters a_x, b_x and k_x the model shows a TI-zone.

TABLE II: Indication which of the discussed models show a TI-zone

	yes	no
IF		x
HH	x	
FH	x	

TABLE III: Indication for which values of the gate parameters there is a TI-zone with a carrier frequency of 3 kHz and a beat frequency of 100 Hz.

	a [1/mV]	b [mV]	k [-]
m	>0.122	>31.32	<1.18
h	<-0.155	<11.58	<1.13
n	<-0.166	<34.21	<1.69

A. IF-models

Figure 2 shows the graphs indicating the threshold lines where a TI signals starts to cause firing at the beat frequency (dashed lines) and where a single sinusoid with the same the carrier frequency as the TI-signal starts causing regular firing (solid lines). With regular firing it is meant that the neuron spikes more than one time during the stimulation pulse. It can be seen that in both the LIF-model and the EIF-model, the single sinusoid causes regular firing at lower input intensities than the TI-signal. For the LIF- model, the dashed blue line is about 2.2 times higher than the red line. For the two EIF-models it is 2.6 and 5 times higher, respectively.
For the AdEx-model, the sinusoidal signal again causes firing at lower intensities (approximatly 3.6 times lower for a sine than for a TI-signal). For all models and all signals, it is clear that for a higher carrier frequency, a higher input is needed to achieve stimulation.

B. Effect non-linearity in current equations

Two methods are used to determine the Taylor expansion points for the gHH and FH1 models, as described in section II-A. For the first method, the expansion points are chosen equal to the Nernst reversal potentials of the ion currents. For the HH-model, this results in $V_{Na0} = 45$ mV and $V_{K0} = -82$ mV. For the FH-model this results in $V_{Na0} = 53.53$ mV, $V_{K0} = -97.74$ mV and $V_{p0} = 53.53$ mV.
For the second method, the average correlations are calculated. The maximum for the FH1v2-model can be found at ($V_{Na,0} = -30.69$ mV, $V_{K,0} = -37.24$ mV) and is equal to 0.994. The average correlation for the FH1v1-model is 0.924. For the gHHv2-model, the maximum is at ($V_{Na,0} = 0.34$ mV, $V_{K,0} =$

-78.6 mV) and is equal to 0.971. The average correlation for the gHH1v1-model is 0.785.

1) FH vs FH1: Figure 3 shows the energy plot of the FH-model and the difference with the energy of the FH1-models ($pTI_{FH} - pTI_{FH1}$) as a comparison. On Figure 3a it can be seen that for a higher f_c value, there is a bigger interval of the input intensity where the neuron reacts at the beat frequency of the TI-input. Also for a higher f_c, a higher input is needed to achieve spiking. From Figures 3b and 3c it can be seen that the behavior of the FH1-models is very similar to the original FH-model. The only difference is that the FH1-models get high energies at the beat frequency at higher input intensities with the FH1v2-model being a closer match to the FH-model. Also the plots of the threshold lines can be used to compare the models. These results are shown in Figure 4. From the threshold lines, the TI-zone can be deduced. Again it can be seen that the models are very alike with some minor differences. Comparing the two dashed lines, the FH-model has a TI-zone up to $f_c = 3.5$ kHz. This changes to a value larger than 4 kHz for the FH1v1 model and 3.2 kHz for the FH1v2 model. The maximal width of the TI-zone is $20\ \frac{\mu\text{A}}{\text{cm}^2}$, $25\ \frac{\mu\text{A}}{\text{cm}^2}$ and $20\ \frac{\mu\text{A}}{\text{cm}^2}$ for the FH, FH1v1 and FH1v2 model, respectively. The FH1v2-model again shows the best match to the FH-model.

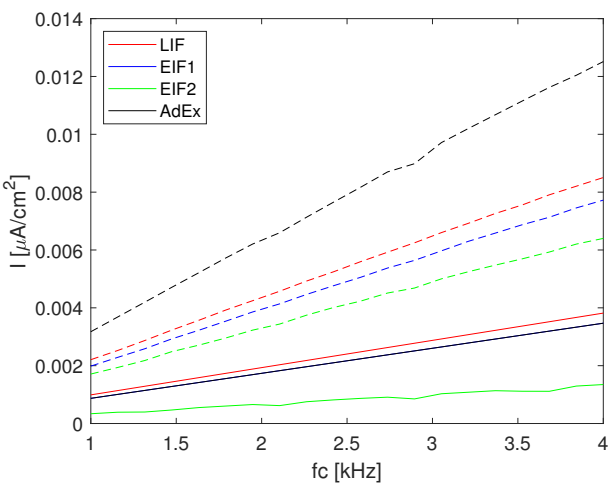

Fig. 2: Threshold lines for regular firing with a sinusoidal input with carrier frequency f_c (solid lines) and firing at the beat frequency (100 Hz) of a TI signal (dashed lines). The thresholds are shown for the leaky integrate-and-fire (LIF), exponential integrate-and-fire with $\Delta_T = 2$ mV (EIF1), exponential integrate-and-fire with $\Delta_T = 15$ mV (EIF2) and adaptive and exponential integrate-and-fire (AdEx) neuron. Note that the solid blue and black line are the same.

2) HH vs gHH: The results for the energy metric and the firing thresholds for the HH- and gHH- models are shown in Figures 5 and 6. From the energy plots it seems like the models again react very similar with only some minor differences due to the approximation. The firing thresholds however suggest that there are big differences with the sine-input. For the sine-input in the HH-model, the neuron never seems to spike above a certain carrier frequency while for the gHH-model, spiking is seen over the whole f_c-range. It is thus possible that the GHK-non-linearity assures more robustness for quickly osillating signals.

C. Gates

1) Time constants: Figure 7 shows the influence of the firing thresholds for the different k-parameters. For the m-gate (Figure 7a), a logarithmic trend is followed. The thresholds increase with increasing k_m-values until it reaches a plateau. Moreover, the blue and red lines cross around $k_m = 1.1$ meaning the TI-zone disappears. With the TI-zone, the region is meant where the TI-signal causes spiking but the single sine does not.

For very low values of k_h (< 0.7), the input intensity needed to achieve spiking increases rapidly for both the TI- and sine- signal for decreasing k_h- values. Around $k_h < 0.1$ it is not possible anymore to create any APs. For $k_h > 0.7$, the threshold current increases for firing at the beat frequency for the TI-input but stays more or less constant for the other threshold lines.

Similar results are found for the n-gate: for very low k_n-values (around $k_n < 1$), all input threshold goes up while for high k_n-values the thresholds stay more or less constant except for firing at the beat frequency.

Finally, it can be seen that the TI-signal is able to cause regular firing at lower input intensities than needed for firing at the

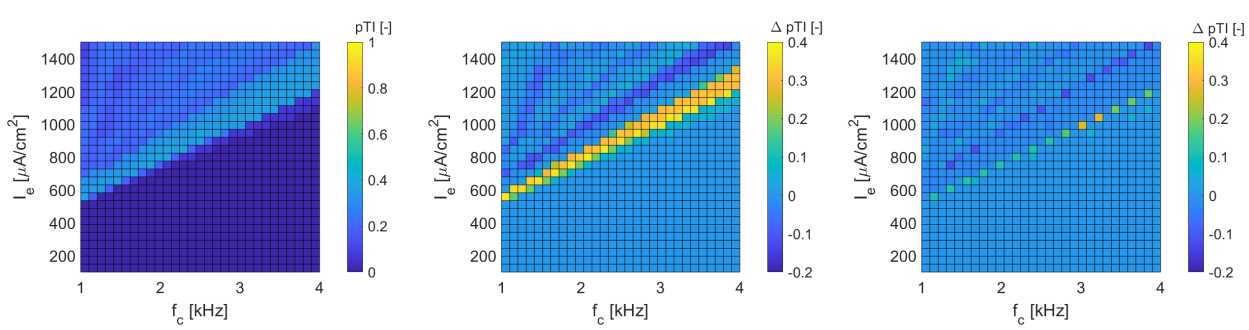

(a) FH-model (b) Difference between FH and FH1v1 (c) Difference between FH and FH1v2

Fig. 3: Comparison of the 2D plot of the energy metric for the FH- and FH1-model with a beat frequency $f_b = 100$ Hz

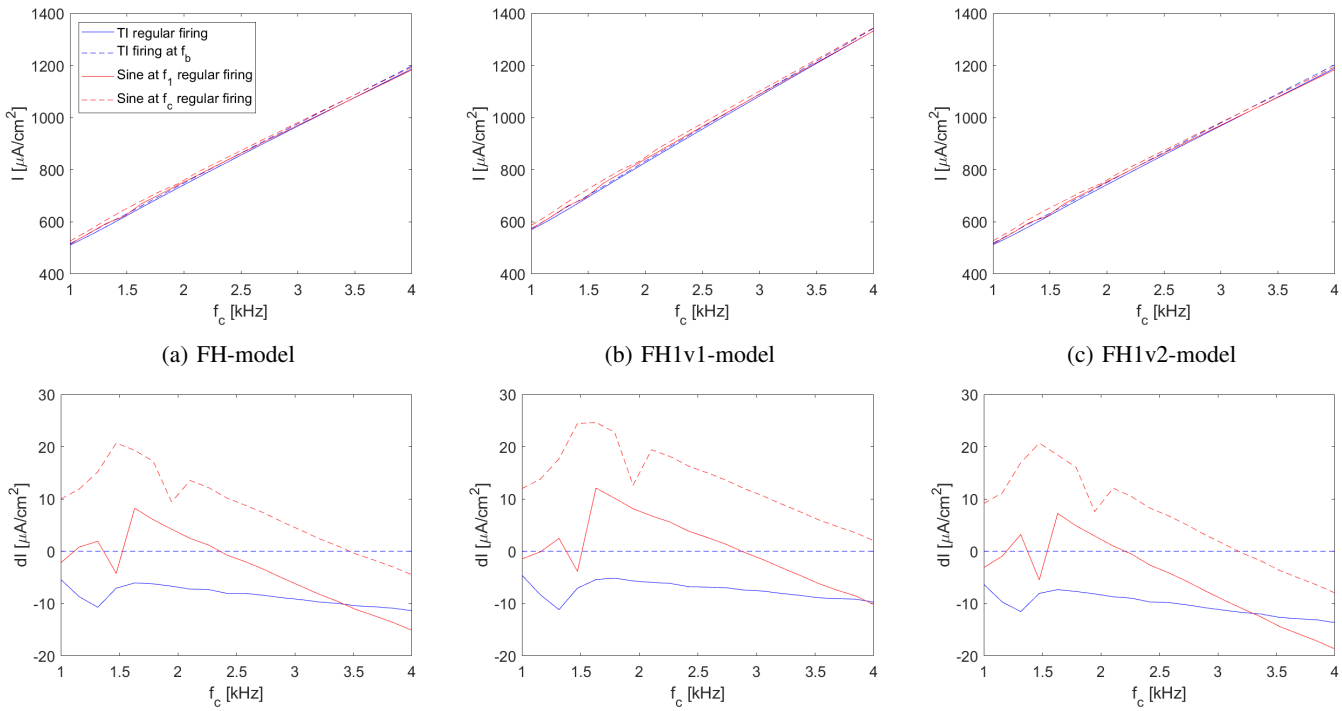

(a) FH-model (b) FH1v1-model (c) FH1v2-model

(d) FH-model (e) FH1v1-model (f) FH1v2-model

Fig. 4: Comparison of the threshold lines for the FH- and FH1-model with a beat frequency $f_b = 100$ Hz. (a)-(c): absolute threshold lines. (d)-(f): relative threshold lines with respect to the threshold line of firing at the beat frequency of the TI-input.

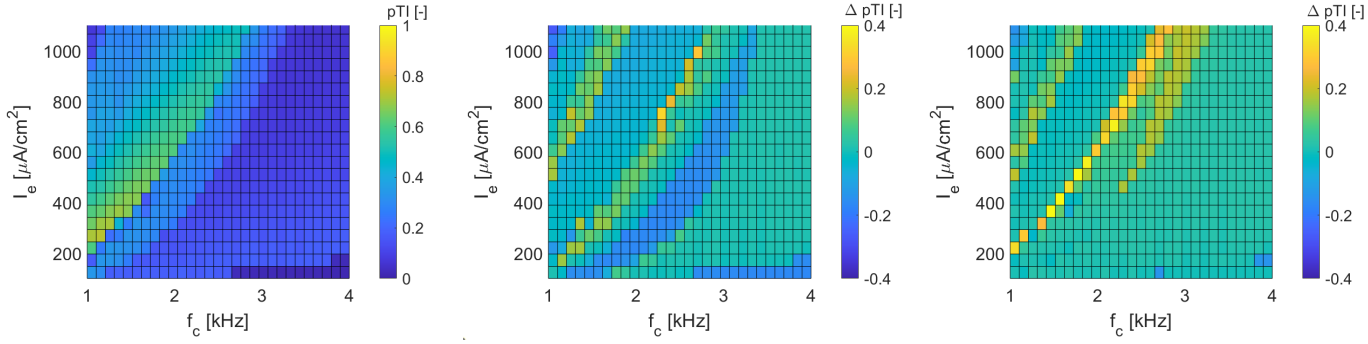

(a) HH-model (b) Difference between HH and gHHv1 (c) [Difference between HH and gHHv2

Fig. 5: Comparison of the 2D plot of the energy metric for the HH- and gHHv1-model with a beat frequency $f_b = 100$ Hz

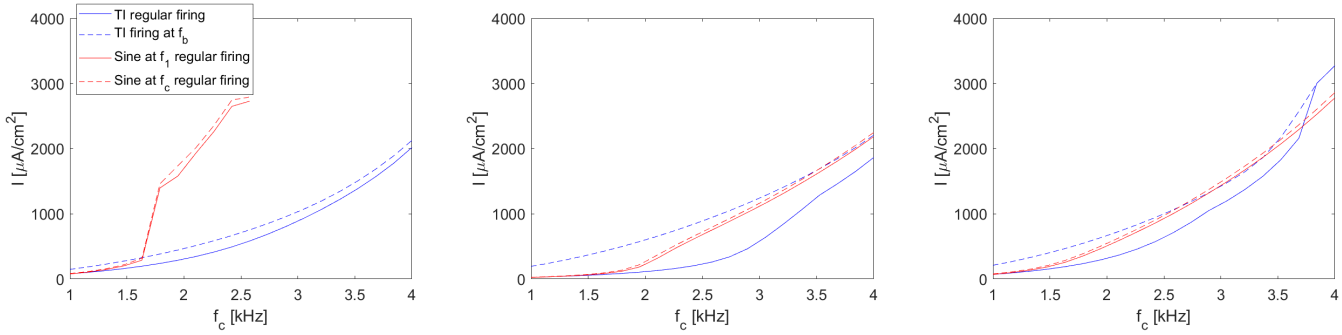

(a) HH-model (b) gHHv1-model (c) gHHv2-model

Fig. 6: Comparison of the threshold lines for the HH- and gHH-model with a beat frequency $f_b = 100$ Hz.

beat frequency. For low k-values, the solid and dashed blue line in Figure 7 are equal or almost equal. A gap of 17.29 $\frac{\mu A}{cm^2}$, 117.0 $\frac{\mu A}{cm^2}$ and 40.38 $\frac{\mu A}{cm^2}$ arises for $k_m = 4$, $k_h = 4$ and $k_n = 4$.

2) Steady state values: The effect of changing the slope of the m-gate's membrane potential dependency is shown in Figure 8a. A higher a-value shifts the TI-zone to higher input currents. The influence of the b-value (i.e. shifting the logistic function along the x-axis) of the m-gate is similar. A small increase in the b-value makes the threshold lines shift to much higher input currents and vice versa. This is depicted in Figure 8b.

For the h-gate, a similar but opposite effect is seen. An increase in b-value makes the TI-zone shift to lower input currents and vice versa (Figure 8d). It has to be noted that this effect is less pronounced. While for the m-gate, a slight change in b-value caused a big shift along the y-axis, for the h-gate a bigger change in b-value is needed to accomplish the same shift. Increasing the a-parameter of the h-gate increases the threshold for spiking activity. In contrast to the m-gate, it increases in a convex way. An interesting observation is that the threshold for the TI-input increases faster than for the sine-input with an intersection of the two dashed lines at $a = -0.15$. Also for the b-parameter, an intersection of blue and red line can be seen at $b = 10$.

For the n-gate, increasing the a-value shifts the threshold lines to lower input currents. This is shown on Figure 8e. For a certain a-value (around $a = 0.15$), there is again an intersection of blue and red line, meaning a disappearance of the TI-zone. The result of the influence on the TI-zone when changing the parameter b is shown in Figure 8b and is analogue to the a-parameter with an intersection around $b = 30$.

IV. Discussion

A. IF models

For all IF-models it was seen that no TI-behavior is present (Figure 2). From the transition from LIF to EIF it is clear that adding a non-linearity is not sufficient to achieve stimulation with the TI-signal at lower intensities than with the single sinusoidal signal. This is in agreement with Cao and Grover (2020) [16]. Moreover, by increasing the effect of the non-linearity ($\Delta_T \uparrow$), it becomes clear that the gap between the thresholds of the sine and TI-signal becomes bigger. From this it can be concluded that in the integratory phase, the sinusoid always reaches the threshold first, even if a non-linear term is added. Also the transition from EIF to AdEx did not show major differences. However, in Esmaeilpour et al. (2021) [17], AdEx neurons did show correspondence with the reality. In that paper they used a network of neurons rather than a single neuron. They also state that the effect was probably seen because they added the slow $\mathrm{GABA_b}$ channels to an existing model so single AdEx neurons probably do not exhibit the TI behavior.

B. Alternative models

From the results of the FH vs FH1 model it became clear that using the Taylor expansion, some small deviations from the original models were seen. Linearising the ion currents thus has some effect on the way the neuron reacts. However, the TI-zone does not disappear as seen with the IF-models. Instead, the TI-zone behaves as an approximation of the more complex model without losing the most important characteristics. Simply adding a non-linearity in the differential equation of the membrane potential is thus not sufficient to fully change the behavior of the neuron model. The reason for the shifts to higher input intensities is because the Na^+-current is lower in magnitude for the FH1-models, so a higher input is needed to achieve firing. This is clarified by the fact that the FH1v2-model is a better approximation and the magnitude of the Na^+-current is higher, especially at the lower membrane potentials.

The comparison of the HH- and gHH- models shows larger differences. However, with both models it is possible to achieve a TI-zone. From this it can be concluded that the GHK non-linearity is not the main reason for a neuron model to show a TI-zone.

C. Gates

The effect of the different characteristics of the gates will be explained in this section, but the mechanism of TI and its responses can be best explained with Figure 9. Figure 9a

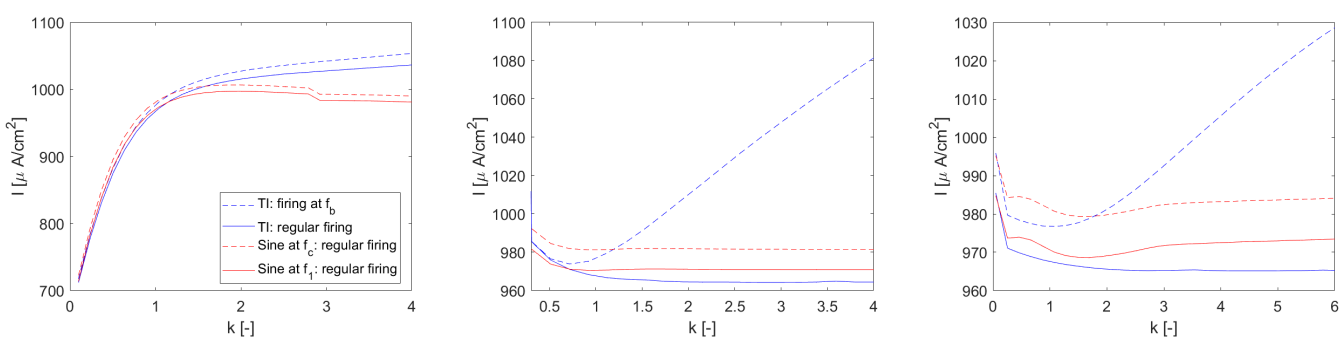

(a) k_m detail (b) k_h detail (c) k_n detail

Fig. 7: Comparison of the threshold lines for different k_x-values

shows that a TI signal can elicit an AP at every other beat, while the sinusoidal signal with the same carrier frequency can only elicit an AP at the stimulation onset. To understand why this is the case, we investigate the gates. For the response to a sinusoidal signal, all the gates reach a state of small-amplitudeos cillations about a quasi-equilibrium value. However, the values where they oscillate are not favorable for neuronal excitation (a higher h-value and a lower n-value would be better). Comparing this to the TI-signal (Figure 9a), it can be seen that because this input signal drops to lower values for a longer period, the n- and h- gates are allowed to return to values that are more favorable to create an AP. This is even more clear in this example where one beat is not able to create an AP because for example the h-gate is still a little too low whereas with the next beat, h is a little higher so the increase of m is able to elicit the AP.

1) Time constants: It was already stated that the m-gate seems to be the gate of which its time constant has the most influence on the behavior of the neuron. For lower time constants, the neuron starts to fire at lower amplitudes of the

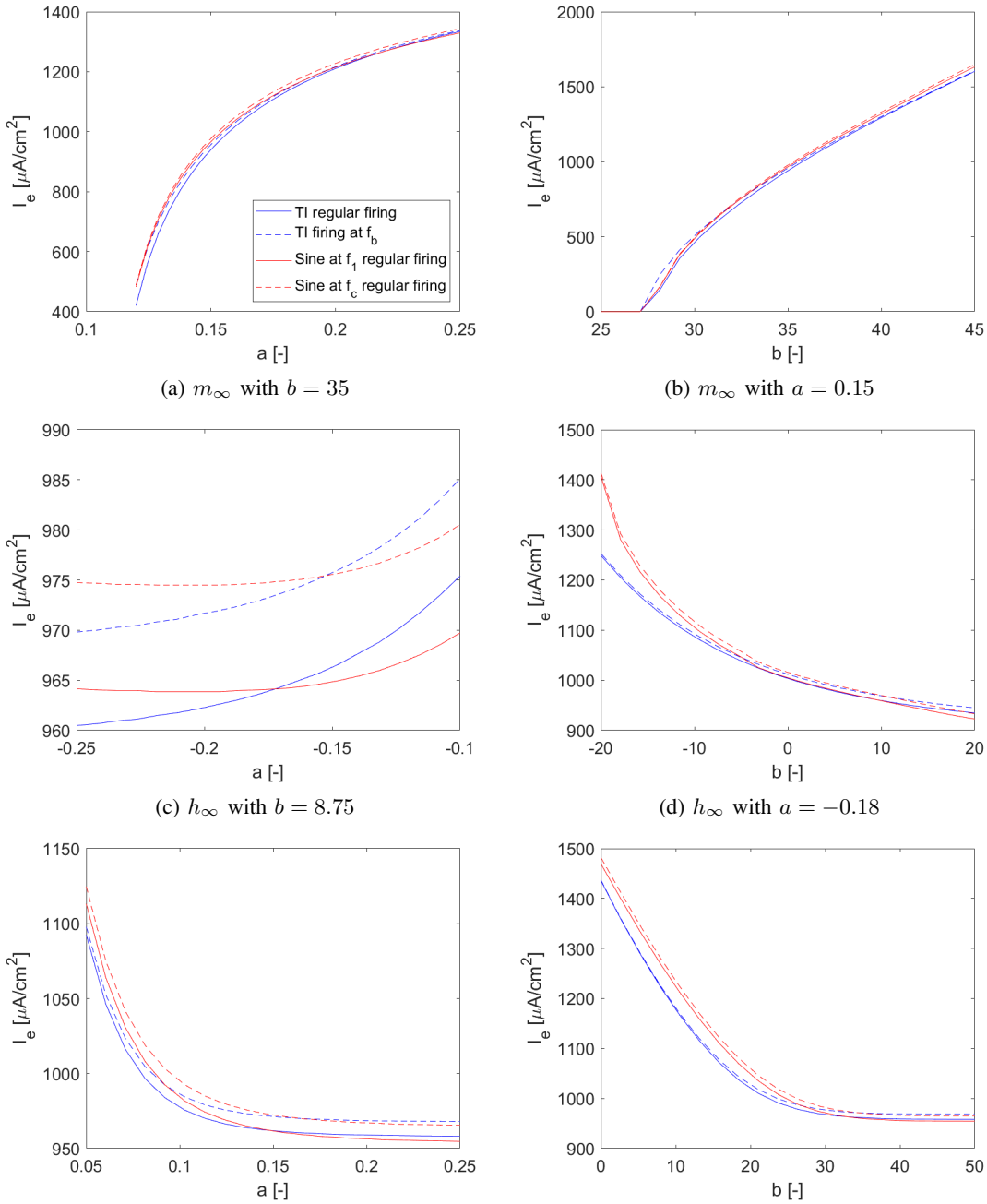

(a) m_∞ with $b = 35$

(b) m_∞ with $a = 0.15$

(c) h_∞ with $b = 8.75$

(d) h_∞ with $a = -0.18$

(e) n_∞ with $b = 30$

(f) n_∞ with $a = 0.12$

Fig. 8: Results for the threshold lines with x_∞ as a logistic function with on one hand a varying a-parameter and constant b-parameter (left) and on the other hand a varying b-parameter and constant a-parameter (right) with $f_c = 3$ kHz and $f_b = 100$ Hz.

input current. This can be explained by the fact that the fast reaction of the m-gate is responsible for the initiation of an AP. Before an AP is formed, the membrane potential will oscillate and, due to the gate equations, so will the gate parameters. Now first imagine that the m-gate would react infinitely fast at the moment an AP should be generated. If then the oscillating membrane potential would reach a certain threshold value causing the m-gate to increase towards a value of 1, an AP will be created instantaneously. For the real situation where the m-gate reacts with a certain lag due to its time constant, the oscillating membrane potential reaches the same value that caused stimulation in the previous example. In this case the m-gate needs some time to react, when this potential is reached, the m-gate will increase. If the potential keeps increasing, the m-gate will also keep increasing and eventually an AP will be created. However, if the potential starts decreasing again shortly after and the m-gate starts decreasing as well, no AP will be created. Because of this, the firing thresholds are at lower input intensities for lower time constants which can be seen in Figure 7a.

For the h-gate it was seen that both very low and very high time constants increase the threshold current. In the case of a very low time constant it is because the h-gate closes too fast. In contrast, high time constants result in reduced h-gate deinactivation after a first action potential, resulting in higher excitation thresholds. This also explains why from a certain point, increasing k_h only has an influence on the threshold for firing at beat frequency of the TI-signal (dashed blue line). The slower the h-gate reacts, the more beats are skipped and the higher the input current has to be to force the neuron to react at every beat. This will not affect the regular firing threshold of the TI-signal because the effect is only on the time between spikes. When the h-gate has reopened, the rapid response of the m-gate will always be able to initiate a new AP, only the FR will be lower. For sine-input, the same reasoning accounts: waiting long enough for the h-gate to reopen will always lead to a new AP, only with a lower FR.

The reasoning for the n-gate is very similar to that of the h-gate because the opening of the n-gates causes an outflow of K^+-ions resulting in a decrease of the membrane potential. Both gates can thus counteract the formation of an AP with the only difference that the effect of the h-gate is multiplicative and the effect of the n-gate is additive.Therefore, a fast reacting n-gate (low k_n) makes it harder to create an AP and thus a higher input current is needed to achieve spiking. For a slower reacting n-gate (high k_n) the n-gate closes too slow so the K^+-outflow is still too high to initiate a new AP at the next beats. The reasoning why the threshold for firing at the beat frequency of the TI-signal changes most with increasing k_n is completely the same as with increasing k_h.

2) Steady state values: From the discussion above it has become clear that the values of the gates play an important role. The time constants that were discussed play a role in how fast the gates can reach a certain value. The steady state characteristic then determines to which value the gates evolve. This is investigate in this study by changing the a- and b-parameters in the logistic function approximation of the gates.

Starting with the m-gate, a TI-zone appears for increasing a- and b-values, although the TI-signal causes regular firing at lower input intensities (Figures 8a and 8b). Changing the steady state values shifts the TI-zone to higher input currents and increases the width of the TI-zone. The reason for the

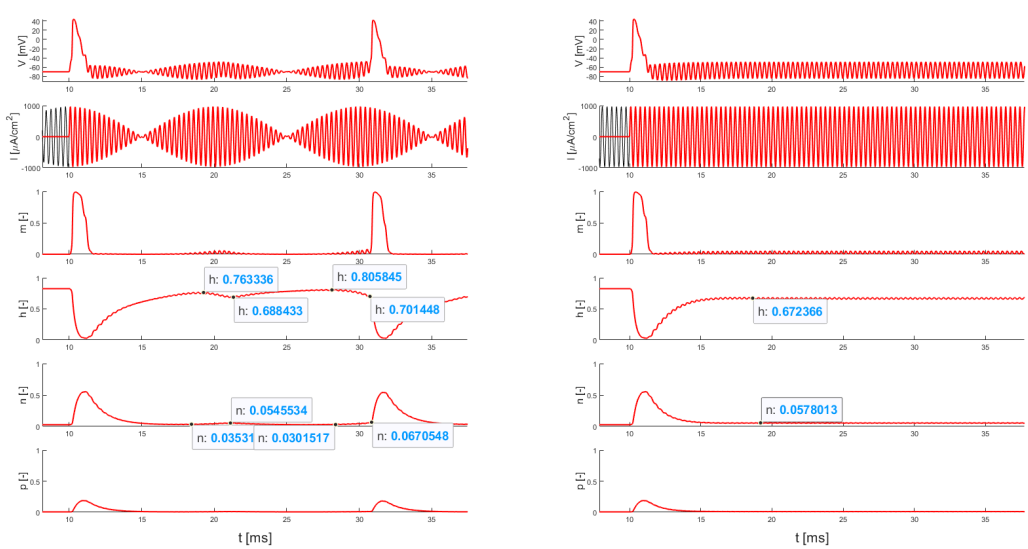

(a) TI-input

(b) Sine-input

Fig. 9: Illustration of the different responses of an FH-neuron to a TI-signal ($f_b = 100$ Hz, $f_c = 3$ kHz and $I_e = 970\ \frac{\mu\text{A}}{\text{cm}^2}$) and a sinusoidal signal ($f = 3$ kHz and $I_e = 970\ \frac{\mu\text{A}}{\text{cm}^2}$)

shift of the threshold to higher input currents is that for a higher a- or b-values, the m-gate is in a more closed state at lower membrane voltages. Interestingly, for values of $b < 27$, the neuron fires spontaneously. In other words, the open probability of the m-gate is high enough at low membrane potentials so the neuron can always enter the positive feedback loop to form an AP.

For the h-gate, the behavior for different values of a and b can basically be explained by the fact that for higher a-values or lower b-values, the h-value around the resting potential is lower. The h-gate is thus already in a more closed state resulting in a lower Na^+-current and a higher input current needed to cause firing.

What is more interesting is that the steepness of the threshold is not the same for the TI-input and the sinusoidal input. For low b-values, this causes a quite big TI-zone, which would be very useful for the application of TI-DBS. The reason for this is the following. When the threshold input is plotted with respect to the beat frequency (Figure 11), it can be seen that a minimum is reached and thus there is an optimal beat frequency to choose for the TI-stimulation. When the characteristic parameters a, b and k of the gates are altered, the minimum shifts to other beat frequencies. For example, inreasing the a- and b-parameter shifts the optimal beat frequencies to lower values. As the optimal f_b comes closer to that a pure sine ($f_b = 0$ Hz) and goes further from the case of $f_b = 100$ Hz, this explains why the red line is less steep compared to the blue line in Figure 8c: due to the increasing a-value, the optimal beat frequency comes closer to that of a sine causing a less steep increase of the threshold. The same holds for the increasing b- parameter in Figure 8d. In this case, the decrease of the red lines is steeper because the sine ($f_b = 0$ Hz) comes closer to the optimal beat frequency with increasing b. On the other hand, the h-value at low membrane voltages increases which is more favorable to create an AP. This means that there is a double effect for the decreasing threshold. For the 100 Hz beat frequency TI-input, the increase in h-value at low membrane potentials for increasing b-value again causes a decrease in threshold but because the optimal beat frequency shifts to lower values, the decrease in threshold is less steep.

The same reasoning can be followed for the m-gate and the n-gate to explain the difference in steepness of the thresholds for the sine and the TI-signal. The reasoning can also be followed for the k-values. In this case, the effect can be best seen for higher k-values in Figure 7: the optimal beat frequency is inversely proportional with k.

The reason for this optimal beat frequency is because of the following: when the beat frequency is too high, some of the gates might not be restored to a value that is sufficient to create a new AP. Because of this, some beats might be skipped in the neuronal response to the TI-waveform. When the beat frequency is too low, the TI-waveform envelope builds up too slow. Because of this slow build up, the h-gate tends to close too fast while the n-gate opens too fast. Because of this the input current needed to create an AP is higher.

Equation (18) can be used to get more insight in the relation between the optimal beat frequency and the membrane channel dynamics. To derive (18), it is assumed that two phases can be distinguished. In each phase τ_x and x_∞ are constant. In the first phase, the gate characteristics take their values at a membrane potential at the peak of the AP. In the second phase, the gate characteristics take their values at a resting potential. This assumption might not be acceptable for the m-gate as its major changes are not with a constant membrane potential

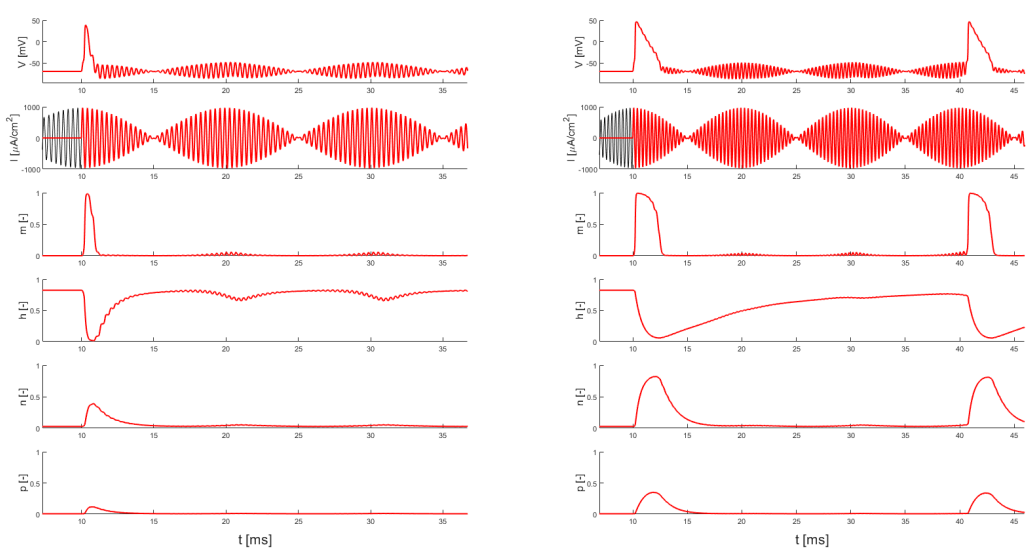

(a) $k_h = 0.5$ (b) $k_h = 3$

Fig. 10: Illustration of the different responses of an FH-neuron to a TI-signal ($f_b = 100$ Hz, $f_c = 3$ kHz and $I_e = 970\ \frac{\mu\text{A}}{\text{cm}^2}$) with different k_h-values

because of its fast nature. A second assumption is that when looking at threshold values, the AP is induced at the top of the beat and the gates should be restored around the node of the TI-signal. A third assumption is that x does not change much in the half period before the AP. This means these two phases should be ran through in a half period of the envelope ($= \frac{1}{2f_b}$).
The starting point in the derivation is (3). With the assumption of a constant τ_x and x_∞, the solution for x during the first and second phase is shown in (15) and (16), respectively.

$$x(t) = (x_0 - x_{\infty,1}) \exp\left(-\frac{t}{\tau_{x,1}}\right) + x_{\infty,1} \tag{15}$$

$$x(t) = (x_1 - x_{\infty,2}) \exp\left(-\frac{t}{\tau_{x,2}}\right) + x_{\infty,2} \tag{16}$$

The next step is to solve $x(t_1) = x_1$ for t_1 and $x(t_2) = x_2$ for t_2. The total time is then the sum of t_1 and t_2:

$$\Delta t = t_1 + t_2 = -\tau_{x,1} \ln\left(\frac{x_1 - x_{\infty,1}}{x_0 - x_{\infty,1}}\right) - \tau_{x,2} \ln\left(\frac{x_2 - x_{\infty,2}}{x_1 - x_{\infty,2}}\right) \tag{17}$$

where x can be h or n. Here, x_0, x_1 and x_2 are the gate parameters at the crest, somewhere between crest and trough (at the minumum of the h-gate or the maximum of the n-gate), and at the through of the envelope, respectively. The optimal beat frequency then becomes:

$$f_{b,optimal} = -\frac{1}{2\left(\tau_{x,1} \ln\left(\frac{x_1 - x_{\infty,1}}{x_0 - x_{\infty,1}}\right) + \tau_{x,2} \ln\left(\frac{x_2 - x_{\infty,2}}{x_1 - x_{\infty,2}}\right)\right)} \tag{18}$$

Because k_x is directly related to the time constant (see (10)), a slower gate means a lower beat frequency is better. The a- and b- parameters are less explicitly included. With a higher a_h, the values of h_0, h_2 and $h_{\infty,2}$ will be lower, h_1 and $h_{\infty,1}$ will be higher. All together, this will result in lower optimal beat frequency. Because of the complexity of the system it is very hard to predict the exact values of h_0, h_1 and h_2. Also, there is an optimal beat frequency for every gate but of course there is only one optimal beat frequency whole system. This should be a combination of the different optima for the different gates. However, (18) still gives some more mathematical insight in why there is an optimal beat frequency and how it depends on the different gate parameters. As an illustration, when the parameters ($h_0 = 0.75$, $h_1 = 0.025$, $h_2 = 0.75$, $h_{\infty,1} = 0$, $h_{\infty,2} = 0.80$, $n_0 = 0.05$, $n_1 = 0.56$, $n_2 = 0.05$, $n_{\infty,1} = 1$ and $h_{\infty,2} = 0.025$) are filled in (18) in the case of spiking at the beat frequency, the resulting optimal beat frequency is 51.1 Hz for the h-gate and 119 Hz for the n-gate. From the simulations it was found to be 52.7 Hz for the whole system. When $k_n = 3$, the optimal beat frequency for the n-gate according to (18) changes to 42.2 Hz while the optimal beat frequency from the simulations is 39.8 Hz. It could thus be argued that the optimal beat frequency of the whole system is largely determined by the slowest gate. However, other effects could still play where the gates cannot be decoupled.

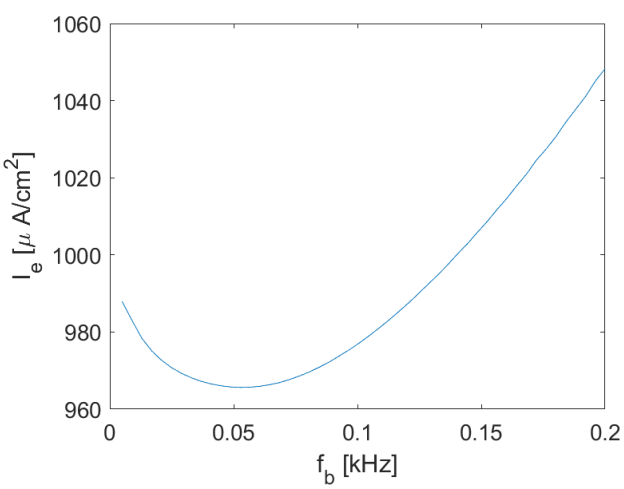

Fig. 11: Illustration of the relation between the threshold for firing at the beat frequency and the beat frequency for the FH-model with $f_c = 3$ kHz

D. Limitations and future work

Because the technique of TI-DBS is quite new, the technique itself can still be improved. It was said in the introduction that the focality of TI-stimulation is in the order of cm. This can be improved by adding extra electrode pairs or by using a sort of lensing effect [24]. Multiple focal points can be achieved by adding extra electrode pairs or by using multiple frequencies in the present electrode pairs. In this way two TI-signals are generated with different carrier frequencies [25]. In classic TI-stimulation, a reference electrode is placed at the chest. ot-TI is a different method where the reference is chosen locally at the brain. This heavily influences the electric field lines. With this method, the importance of the direction of the electric field can be shown [26].
In the study of the underlying mechanism, it can be considered to investigate more morphologically correct neurons to include propagation of the signal through a neuron. It can also be interesting to look at a network of neurons to include the influence of synapses. Lastly, in this study the stimulation due to the electric field is directly translated into an input current into the neuron. In reality, one should look at the activation function due to this electric field. This is expected to further improve our understanding of temporal interference stimulation.

V. Conclusion

This study consists of two major parts. First, the discussion of the complexity of neuron models needed to be able to model experimentally observed response to TI-DBS. The second part focuses on the biophysics of the ion-gates in relation to TI-stimulation.
From the first part it can be concluded that the non-linearity in the GHK-equation alone is not able to explain the underlying mechanism of TI-DBS. For the FH-model, the linearisation causes some minor differences in the neuronal response, that

are not sufficient to describe the TI underlying mechanism. For the HH-model, the differences caused by the GHK non-linearity are bigger. However, the Hodgkin-Huxley TI-zone is actually larger in the linearised model, confirming that the GHK non-linearity is not necessary in order to observe neuronal sensitivity to a beating sine. It should be noted that the choice of the expansion points has a big influence on the behavior as well. From the investigation of the IF-models it can also be concluded that the introduction of a non-linear term in the differential equations is not able to shift the threshold of the TI-input beneath that of the sinusoidal input.

From the second part, it can be concluded that the non-linearities of the gates have a big influence on how the neurons react to the TI- and sine-input. The mechanism is a complex interplay between the gates that driven by the gate characteristics in terms of the time constants and steady state values. This paper showed that changing the gate characteristics can influence the existance and the width of the TI-zone. A TI-zone can appear with increasing a_m- and b_m- values or with a decrease of the other a_x, b_x and k_x parameters. It was also shown that for a certain neuron, it is possible to find the optimal stimulation parameters to increase the TI-zone. This is an interesting finding for the optimization of TI-DBS, where there is a combination of different neuron types at different locations throughout the brain.

VI. Acknowledgements

We want to thank Michiel De Kesel for the exploratory work and discovering the possible importance of the non-linearity of the GHK-equation.

VII. Conflict of interests

The authors declare that there is no conflict of interest regarding the publication of this paper.

References

[1] D. J. Aum and T. S. Tierney, "Deep brain stimulation: foundations and future trends," *Frontiers in Bioscience*, vol. 23, no. 1, pp. 162–182, 2018.

[2] N. Grossman, D. Bono, N. Dedic, S. B. Kodandaramaiah, A. Rudenko, H. J. Suk, A. M. Cassara, E. Neufeld, N. Kuster, L. H. Tsai, A. Pascual-Leone, and E. S. Boyden, "Noninvasive deep brain stimulation via temporally interfering electric fields," *Cell*, vol. 169, pp. 1029–1041.e16, 6 2017.

[3] N. Grossman *et al.*, "Translating temporal interference brain stimulation to treat neurological and psychiatric conditions," *JAMA Neurology*, vol. 75, no. 11, pp. 1307–1308, 2018.

[4] S. Song, J. Zhang, Y. Tian, L. Wang, and P. Wei, "Temporal interference stimulation regulates eye movements and neural activity in the mice superior colliculus¡sup¿*¡/sup¿," in *2021 43rd Annual International Conference of the IEEE Engineering in Medicine Biology Society (EMBC)*, 2021, pp. 6231–6234.

[5] M. D. Sunshine, A. M. Cassarà, E. Neufeld, N. Grossman, T. H. Mareci, K. J. Otto, E. S. Boyden, and D. D. Fuller, "Restoration of breathing after opioid overdose and spinal cord injury using temporal interference stimulation," *Communications Biology*, vol. 4, 12 2021.

[6] X. Su, J. Guo, M. Zhou, J. Chen, L. Li, Y. Chen, X. Sui, H. Li, and X. Chai, "Computational modeling of spatially selective retinal stimulation with temporally interfering electric fields," *IEEE Transactions on Neural Systems and Rehabilitation Engineering*, vol. 29, pp. 418–428, 2021.

[7] M. M. Sorkhabi, K. Wendt, and T. Denison, "Temporally interfering tms: Focal and dynamic stimulation location," vol. 2020-July. Institute of Electrical and Electronics Engineers Inc., 7 2020, pp. 3537–3543.

[8] Z. Xin, A. Kuwahata, S. Liu, and M. Sekino, "Magnetically induced temporal interference for focal and deep-brain stimulation," *Frontiers in Human Neuroscience*, vol. 15, 9 2021.

[9] J. von Conta, F. H. Kasten, B. Ćurčić Blake, A. Aleman, A. Thielscher, and C. S. Herrmann, "Interindividual variability of electric fields during transcranial temporal interference stimulation (ttis)," *Scientific Reports*, vol. 11, 12 2021.

[10] S. Rampersad, B. Roig-Solvas, M. Yarossi, P. P. Kulkarni, E. Santarnecchi, A. D. Dorval, and D. H. Brooks, "Prospects for transcranial temporal interference stimulation in humans: A computational study," *NeuroImage*, vol. 202, 11 2019.

[11] J. Gomez-Tames, A. Asai, and A. Hirata, "Multiscale computational model reveals nerve response in a mouse model for temporal interference brain stimulation," *Frontiers in Neuroscience*, vol. 15, 6 2021.

[12] Y. Huang and L. C. Parra, "Can transcranial electric stimulation with multiple electrodes reach deep targets?" pp. 30–40, 1 2019.

[13] Y. Huang, A. Datta, and L. C. Parra, "Optimization of interferential stimulation of the human brain with electrode arrays," *Journal of Neural Engineering*, vol. 17, 6 2020.

[14] E. Mirzakhalili, B. Barra, M. Capogrosso, and S. F. Lempka, "Biophysics of temporal interference stimulation," *Cell Systems*, vol. 11, pp. 557–572.e5, 12 2020.

[15] P. G. Jiaming Cao, "Do single neuron models exhibit temporal interference stimulation?" *2018 IEEE Biomedical Circuits and Systems Conference (BioCAS)*, pp. 1–4, 2018.

[16] J. Cao, B. Doiron, C. Goswami, and P. Grover, "The mechanics of temporal interference stimulation," *bioRxiv*, 2020.

[17] Z. Esmaeilpour *et al.*, "Temporal interference stimulation targets deep brain regions by modulating neural oscillations," *Brain Stimulation*, vol. 14, no. 1, pp. 55–65, 2021.

[18] B. Howell and C. C. McIntyre, "Feasibility of interferential and pulsed transcranial electrical stimulation for neuromodulation at the human scale," *Neuromodulation*, vol. 24, pp. 843–853, 7 2021.

[19] A. L. Hodgkin and A. Huxley, "A quantitative description of membrane current and its application to conduction and excitation in nerve," *Journal of Physiology*, vol. 117, no. 1, pp. 500–544, 1952.

[20] B. Frankenhaeuser and A. Huxley, "The action potential in the myelinated nerve fibre of xenopus laevis ad computed on the basis of voltage clamp data," *Journal of Physiology*, vol. 171, no. 1, pp. 302–315, 1964.

[21] R. Brette and W. Gerstner, "Adaptive exponential integrate-and-fire model as an effective description of neuronal activity," *Journal of Neurophysiology*, vol. 94, no. 1, pp. 3637–3642, 2005.

[22] Mathworks, "Solver," 2021, https://nl.mathworks.com/help/simulink/gui/solver.html.

[23] M. N. R. Ashino and R. Vaillancourt, "Behind and beyond the matlab ode suite," *Computers & Mathematics with Applications*, vol. 40, no. 4, pp. 491–512, 2000.

[24] J. Cao and P. Grover, "Stimulus: Noninvasive dynamic patterns of neurostimulation using spatio-temporal interference," *IEEE Transactions on Biomedical Engineering*, vol. 67, pp. 726–737, 3 2020.

[25] X. Zhu, Y. Li, L. Zheng, B. Shao, X. Liu, C. Li, Z. G. Huang, T. Liu, and J. Wang, "Multi-point temporal interference stimulation by using each electrode to carry different frequency currents," *IEEE Access*, vol. 7, pp. 168 839–168 848, 2019.

[26] F. Missey, E. Rusina, E. Acerbo, B. Botzanowski, A. Trébuchon, F. Bartolomei, V. Jirsa, R. Carron, and A. Williamson, "Orientation of temporal interference for non-invasive deep brain stimulation in epilepsy," *Frontiers in Neuroscience*, vol. 15, 6 2021.